Supporting Information

Dimensionality-Regulated Hofmann MOFs Derived 3D Core–Shell CoNi/C Composites for High-Performance Broadband Microwave Absorption

Hongdu Jin*[a], Jun Lin[b], Yaoyao He[c], Guangyong Pan[a], Jun Lv[a], Yongjie Qi[a], Chengyu Huang[a], Fei Wang[a], and Hui-Min Wen*[b]

[a] College of Intelligent Manufacturing, Zhejiang Guangsha Vocational and Technical University of Construction, Jinhua 322100, P.R. China.

[b] College of Chemical Engineering, Zhejiang University of Technology, Hangzhou 310014, P.R. China

[c] Zhejiang Pengcheng Technology Co., Ltd., Jinhua 322100, P.R. China.

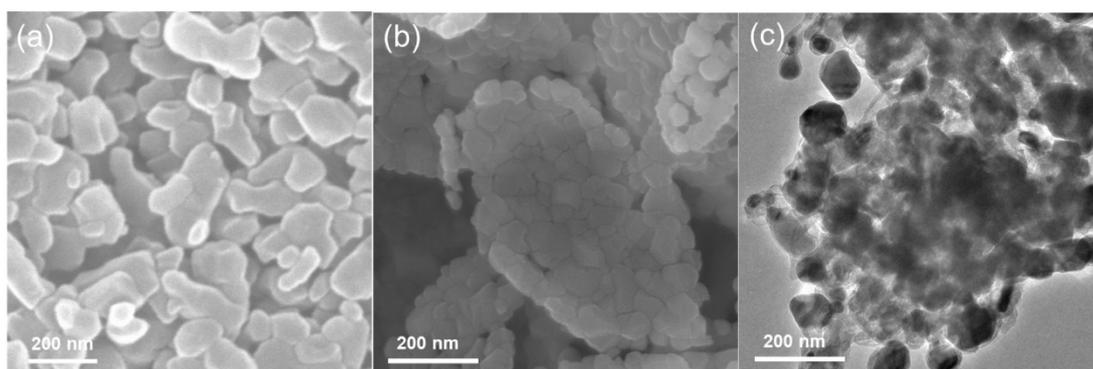E-mail: jinhongdu@zjgsdx.edu.cn, huiminwen@zjut.edu.cn

Fig.S1. (a) SEM image of Hofmann MOF; (b) SEM image and (c) TEM images of P-700.
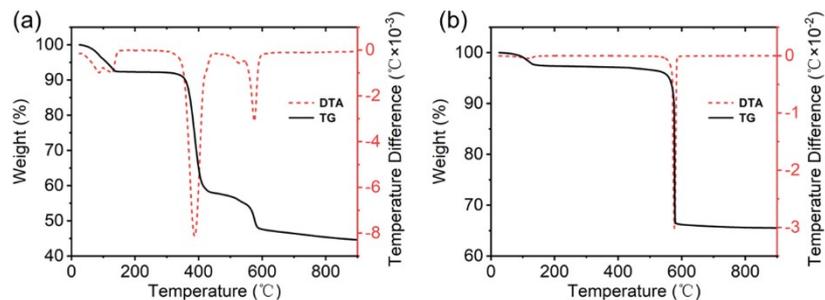
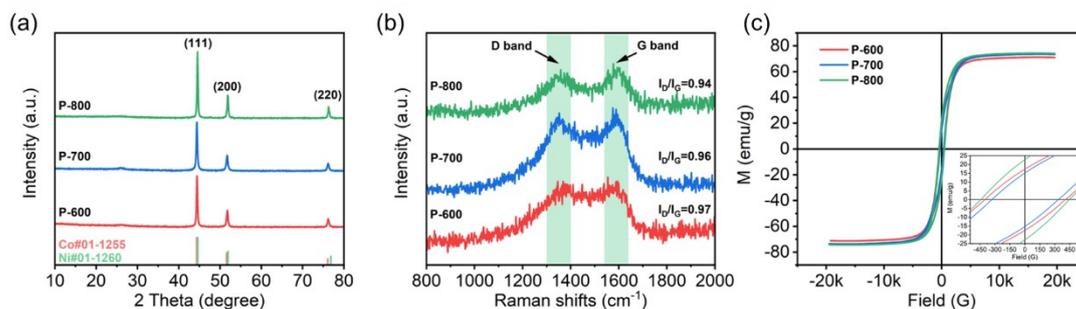**Fig.S2.** TG and DTA patterns of (a) Hofmann MOF and (b) Co[Ni(CN)4].

Fig.S3. (a) XRD patterns, (b) Raman patterns and (c) hysteresis loop of P-600, P-700 and P-800.

Table S1. Content of each element of Hofmann-700 and P-600

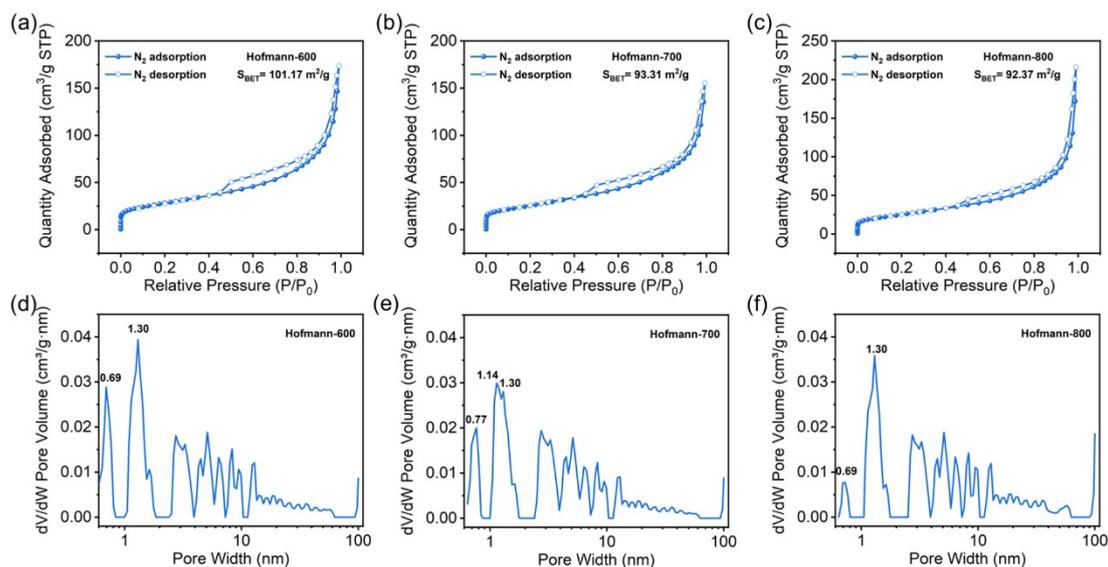| Sample	C/wt%	O/wt%	Co/wt%	Ni/wt%
Hofmann-700	14..9	1.1	44.9	39.1
P-600	8.2	0.5	51.8	39.5

Fig.S4. N$_2$ absorption-desorption isotherm and pore-size distribution of (a, d) Hofmann-600, (b, e) Hofmann-700 and (c, f) Hofmann-800.
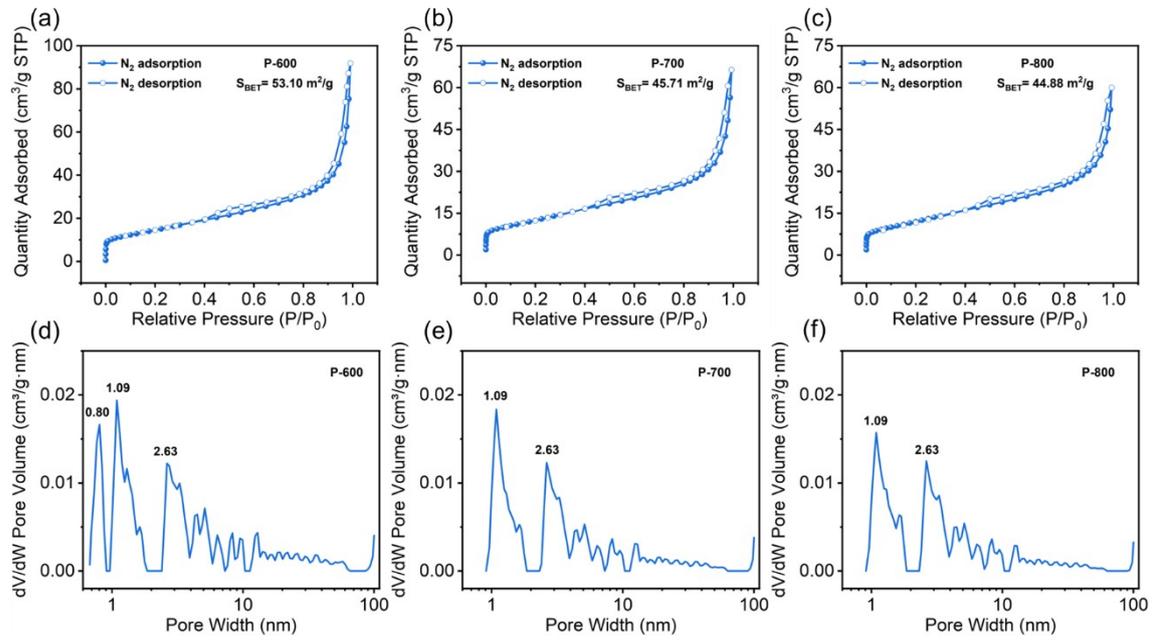
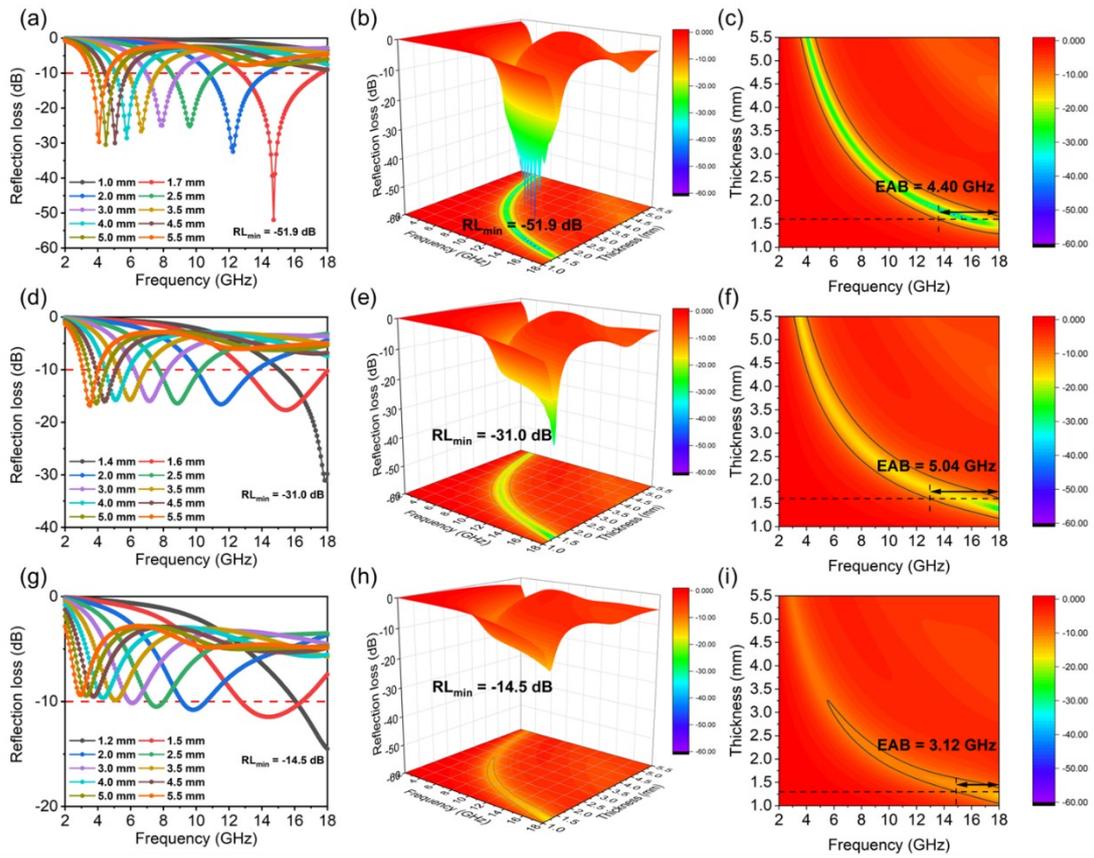**Fig.S5.** N₂ absorption-desorption isotherm and pore-size distribution of (a, d) P-600, (b, e) P-700 and (c, f) P-800.

Fig.S6. RL, 3D RL and 2D RL of (a, b, c) P-600, (d, e, f) P-700 and (g, h, i) P-800.
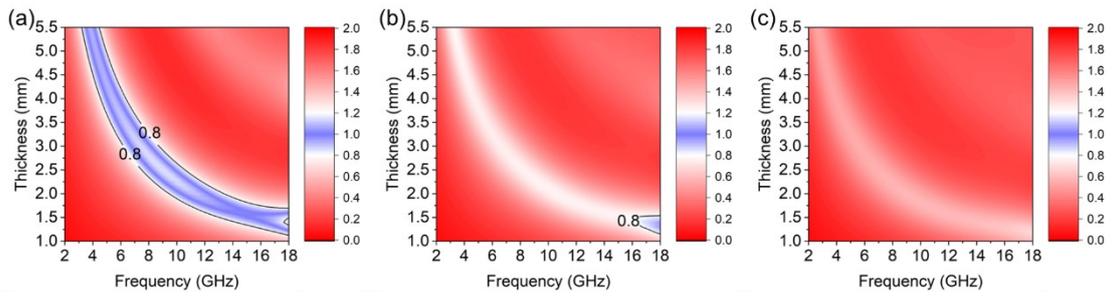
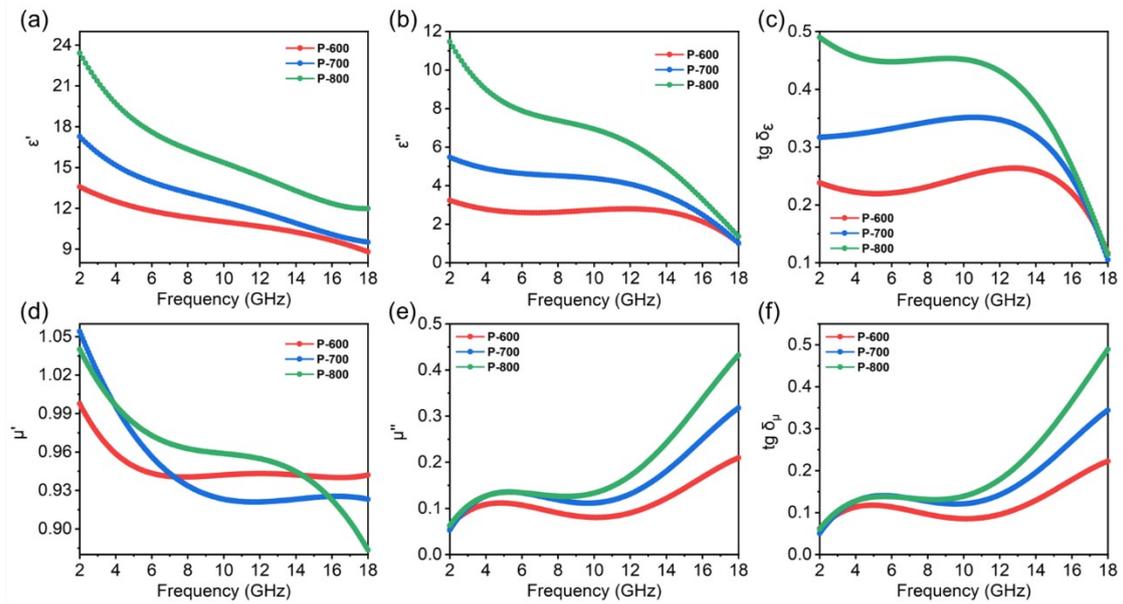**Fig.S7.** 2D impedance matching of (a) P-600, (b) P-700 and (c) P-800.

Fig.S8. (a) Permittivity real part ε', (b) permittivity imaginary part ε", (c) dielectric loss tangent tanδε, (d) permeability real part μ', (e) permeability imaginary part μ", and (f) magnetic loss tangent tanδμ of P-600, P-700 and P-800.
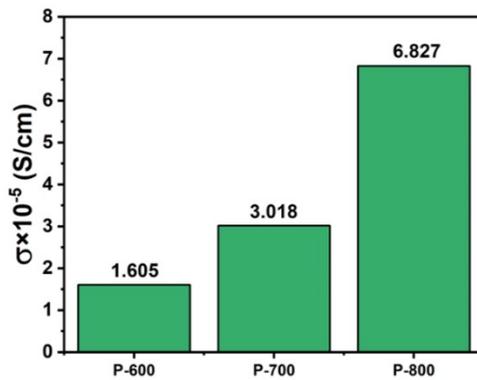

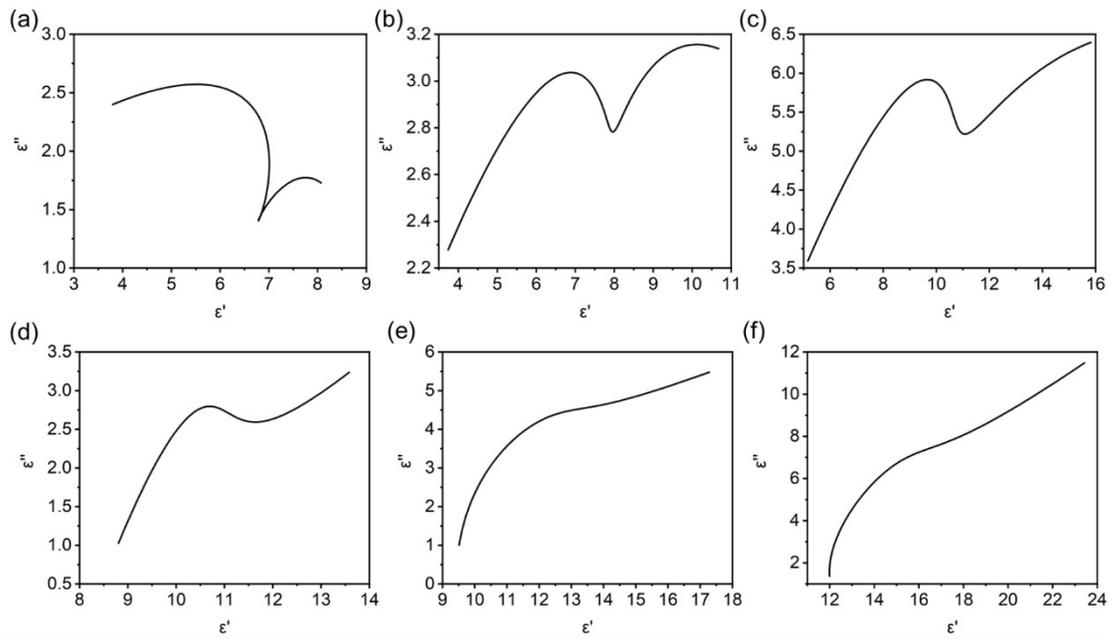**Fig.S9.** Conductivity of Co[Ni(CN)4] derivatives P-X.

Fig.S10. The Cole-Cole plots of (a) Hofmann-600, (b) Hofmann-700, (c) Hofmann-800, (d) P-600, (e) P-700 and (f) P-800.
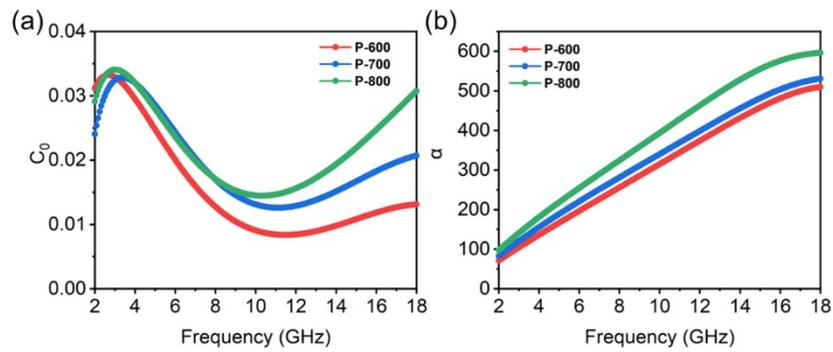

Fig.S11. (a) C_0 curves, (b) attenuation constant of P-600, P-700 and P-800.